AAPS PharmSciTech, Vol. 12, No. 1, March 2011 (© 2011)
DOI: 10.1208/s12249-010-9576-8

Research Article

A Composite Polyelectrolytic Matrix for Controlled Oral Drug Delivery

Priya Bawa,[1] Viness Pillay,[1,2] Yahya Essop Choonara,[1] Lisa Claire du Toit,[1] Valence Methaius Kessy Ndesendo,[1] and Pradeep Kumar[1]

Received 7 September 2010; accepted 16 December 2010; published online 12 January 2011

Abstract. The purpose of this study was to formulate drug-loaded polyelectrolyte matrices constituting blends of pectin, chitosan (CHT) and hydrolyzed polyacrylamide (HPAAm) for controlling the premature solvation of the polymers and modulating drug release. The model drug employed was the highly water-soluble antihistamine, diphenhydramine HCl (DPH). Polyelectrolyte complex formation was validated by infrared spectroscopy. Matrices were characterized by textural profiling, porositometry and SEM. Drug release studies were performed under simulated gastrointestinal conditions using USP apparatus 3. FTIR spectra revealed distinctive peaks indicating the presence of $-COO^-$ symmetrical stretching (1,425–1,390 cm^{-1}) and $-NH_3^+$ deformation (1,535 cm^{-1}) with evidence of electrostatic interaction between the cationic CHT and anionic HPAAm corroborated by molecular mechanics simulations of the complexes. Pectin–HPAAm matrices showed electrostatic attraction due to residual $-NH_2$ and $-COO^-$ groups of HPAAm and pectin, respectively. Textural profiling demonstrated that CHT-HPAAm matrices were most resilient at 6.1% and pectin–CHT–HPAAm matrices were the least (3.9%). Matrix hardness and deformation energy followed similar behavior. Pectin–CHT–HPAAm and CHT–HPAAm matrices produced type IV isotherms with H3 hysteresis and mesopores (22.46 nm) while pectin–HPAAm matrices were atypical with hysteresis at a low P/P_0 and pore sizes of 5.15 nm and a large surface area. At $t_{2\ h}$, no DPH was released from CHT–HPAAm matrices, whereas 28.2% and 82.2% was released from pectin–HPAAm and pectin–CHT–HPAAm matrices, respectively. At $t_{4\ h}$, complete DPH release was achieved from pectin–CHT–HPAAm matrices in contrast to only 35% from CHT–HPAAm matrices. This revealed the release-modulating capability of each matrix signifying their applicability in controlled oral drug delivery applications.

KEY WORDS: composite polyelectrolytes; controlled oral drug delivery; hydrolyzed polyacylamide; matrix characterization; polysaccharides.

INTRODUCTION

As the biomedical and biotechnological sciences make huge strides in advancing drug delivery technology, increased pressure is being placed on the development of novel polymeric materials derived from natural polymers. An effective and simple means of creating these new materials is by a process termed "blending". Blends of "natural–natural" polymers and "synthetic–synthetic" polymers have been widely investigated. Even though natural polymers may possess superior biocompatibility, their mechanical properties are often unsatisfactory (1). On the other hand, synthetic polymers have desirable mechanical properties and only satisfactory biocompatibility. Therefore, blends of natural–synthetic polymers are targeted as a more efficacious means of meeting the needs of modern materials science (2–5). Chemically modified natural polysaccharides have shown diverse potential due to their enhanced hydrophilic properties and their intrinsic polyelectrolyte character (6–8). The latter characteristic provides for the electrostatic interaction between two oppositely charged polyelectrolytes when blended in aqueous solutions to form what is known as polyelectrolyte complexes (PECs) (7–11). These PECs have been shown to exhibit unique physical and chemical properties due to the considerably stronger electrostatic interactions compared to most other secondary binding interactions (12). Oppositely charged polysaccharides are also capable of interacting in the same manner and considering their numerous desirable properties such as their biodegradability, biocompatibility, hydrophilicity and protective properties, increased interest is being placed on them (13–15). A variety of polysaccharide-based PECs have been formulated and evaluated for diverse applications (16–20). Among their numerous benefits, these complexes are also capable of providing a greater barrier to drug release in the upper gastrointestinal tract than either material alone.

Polyacrylamide (PAAm) is a water-soluble non-ionic synthetic polymer typically obtained by free radical polymerization of acrylamide in an aqueous medium (21). It is generally used as a strengthening agent, an erosion-prevent-

[1] Department of Pharmacy and Pharmacology, University of the Witwatersrand, 7 York Road, Parktown, 2193 Johannesburg, South Africa.
[2] To whom correspondence should be addressed. (e-mail: viness.pillay@wits.ac.za)

ing and infiltration-enhancing polymer. It is also commonly applied in gel electrophoresis (22–24). Transformation of the essentially neutral PAAm molecule into a strong anionic molecule is generally achieved as a consequence of hydrolysis which results in a partially hydrolyzed PAAm (HPAAm) molecule due to the partial conversion of its amide groups to carboxylate groups (25). Therefore when in aqueous solution, this polymer presents with a polyelectrolyte character. The fundamental process of HPAAm synthesis is based on a so-called simultaneous polymerization–hydrolysis process whereby the hydrolysis reaction of PAAm is conducted concurrently with the polymerization of the acrylamide (26). The most prevalent means of HPAAm formation is by alkaline hydrolysis of PAAm using hydrolyzing agents such as alkali metal carbonates, alkali metal hydroxides, alkali metal sulfates, or alkali metal chlorides (27).

Chitosan (CHT) is a partially de-acetylated derivative of chitin which possesses unique physicochemical and biological properties such as an enhanced biocompatibility and antimicrobial capability. However apart from these factors, its cationic nature and high-charge density in solution along with its mucoadhesive properties has made it one of the most popular natural polymers for use in oral controlled drug delivery technology (28). In addition, the ability of CHT to form non-covalent complexes with other polyelectrolytes (bio-polyelectrolytes, modified natural polyanions, or synthetic polyanions) adds to its attractiveness for use in controlled drug delivery (29).

Pectin, a naturally occurring anionic polysaccharide has also been greatly explored for its potential in drug delivery technology, especially for targeted colonic delivery (30–34). However, the high hydrophilicity of pectin warrants the need to identify methods of effectively reducing the premature solubility while maintaining its polymeric backbone. By polyelectrolyte complexation of this phyto-polysaccharide with CHT, the intrinsic beneficial properties of pectin can be maintained while allowing a reduction in the hydrophilicity thus facilitating its use in many controlled release drug delivery systems (16,35). In addition, the susceptibility of polysaccharide polymers to colonic enzymatic degradation may be enhanced by reducing the premature solvation of the relevant polymer in the upper gastrointestinal tract, thus facilitating a more targeted and site-specific delivery of pharmaceutical agents in the distal small intestine and colon.

Accordingly, the present study focused on the formulation of a lyophilized polyelectrolyte matrix constituting combinations of natural polymers such as pectin and CHT and a partially hydrolyzed synthetic polymer, HPAAm derived from polyacrylamide. This formulation approach was aimed at the facilitation of a reduction in the premature solvation of the polysaccharide polymer, either CHT or pectin or a combination thereof, in turn reducing upper gastrointestinal release of the model highly water-soluble drug, diphenhydramine HCl (DPH), and providing an intact matrix for entry in the colon. DPH was employed as the model drug to prove the modulating effect of the lyophilized polyelectrolyte matrix on drug release. The matrix was investigated for its *in vitro* drug release characteristics under conditions simulating the gastric and small intestinal environments. Furthermore, the matrices also underwent intensive physicomechanical and physicochemical analysis, with the aim of determining the textural parameters of matrix resilience, matrix hardness and deformation energy. Fourier transmission infrared spectroscopy (FTIR) was performed to elucidate the successful synthesis of the polyelectrolyte matrix of the relevant polymers and was corroborated by Molecular Mechanics simulations. Pore structure, distribution, and volume were elucidated based on the Barrett, Joyner, and Halenda (BJH) theory (36) and was then correlated with the microscopic architecture of the matrices. The Brunauer–Emmett–Teller (BET) theory (37) of surface area determination was then employed for matrix evaluation.

MATERIALS AND METHODS

Materials

The natural polysaccharide polymers employed included CHT (food grade powder) (Wellable Group Marine Biological & Chemical Co., Ltd., Shishi City, Fujian, China) and pectin (Classic Cu 701; DE: 34–38%; Herbstreith & Fox KG, Neuenbürg, Baden-Württemberg, Germany) of molecular weights (M_w) 160.9 and 70,000 g/mol, respectively. PAAm ($M_w = 5\times10^6$–6×10^6 g/mol), the synthetic non-ionic polymer, was purchased from Fluka Biochemika (St. Louis, MO, USA) and glacial acetic acid was acquired from Rochelle Chemicals (Johannesburg, Gauteng, South Africa). Sodium persulphate (SPS) (SigmaUltra, minimum 98%) as the hydrolyzing agent was purchased from Sigma-Aldrich (St. Louis, MO, USA) and N,N,N′,N′-tetramethylethylenediamine (TEMED; absolute ≥ 99%, GC) as the accelerant was purchased from Fluka (Buchs, AG, Switzerland). DPH with a water solubility of 100 mg/mL at 25°C was employed as the model drug and was purchased from Sigma-Aldrich-Chemie GmbH (Steinheim, Luxembourg, Germany). All materials employed were of analytical grade and used without further purification.

Synthesis of the Composite Polyelectrolyte Matrices

Three formulations consisting of various combinations of the polysaccharide (CHT and/or pectin) and PAAm were synthesized (Table I). Briefly, a 10%$^{w}/_{v}$ aqueous solution of the relevant polysaccharide was blended with a 5%$^{w}/_{v}$

Table I. Composition of Each Lyophilized Polyelectrolyte Matrix Formulation

Formulation	Polymer type	Concentration (%$^{w}/_{v}$)	Volume ratio ($^{v}/_{v}$)	SPS[a]/TEMED[b] ($^{w}/_{v}$)
1	CHT/HPAAm	10:5	2:1	4:1
2	Pectin/HPAAm	10:5	2:1	4:1
3	Pectin/CHT/HPAAm	10:10:5	1:1:1	4:1

[a] Sodium persulfate (hydrolyzing agent)
[b] N,N,N′,N′-Tetramethylethylenediamine (accelerant)

solution of PAAm in a 2:1 ($^{v}/_{v}$) ratio. All solutions were agitated until a visibly homogenous solution was obtained. DPH was then dissolved into the homogenous blend and was further agitated to facilitate a uniform distribution of the drug. Hydrolization of PAAm was permitted with the addition of SPS, in conjunction with TEMED as an accelerant in a 4:1 ratio. The reaction was allowed to proceed under constant agitation at 25°C for 3 h. Matrices consisting of pectin, CHT and HPAAm were prepared in an identical manner as described above and in the same concentrations. However, all three polymers were used in equal volumes, *i.e.*, in a 1:1:1 ratio. After 3 h of constant agitation, the polyelectrolyte blends were subjected to dialysis through 12,000–14,000 Da Dialysis Tubing (cellulose tube, average fiat width 25 mm) (Sigma Chem. Co., MO, USA). After dialysis, 1 mL aliquots of each polyelectrolyte blend was pipetted into pre-lubricated cylindrical molds (13×5 mm) and were subsequently frozen at −70°C for 24 h prior to lyophilization (FreeZone® 2.5, Labconco®, Kansas City, Missouri, USA) at 25 mtorr for 48 h. Lyophilization of the polyelectrolyte DPH-loaded blends was performed with the aim of removing excess solvent involved in the hydrolysis and complexation process, thus ensuring a more stable and robust formulation of defined dimensions.

Elucidation of the Structural Variations of the Polyelectrolyte Matrices

FTIR was performed on all native polymers involved in matrix formulation as well as on the lyophilized matrices as a means of validating the successful synthesis of the polyelectrolyte complex between HPAAm and the relevant polysaccharides. A Perkin Elmer Spectrum 2,000 FTIR spectrometer with a MIRTGS detector, (PerkinElmer Spectrum 100, Llantrisant, Wales, UK) was employed for analysis. Samples were placed on a diamond crystal and processed by universal ATR polarization accessory for the FTIR spectrum series at a resolution of 4 cm^{-1}. Samples were analyzed at wave numbers ranging from 400 to 4,000 cm^{-1}.

Chemometric Molecular Mechanics Simulations

All modeling and computations, including energy minimizations in molecular mechanics, were performed using HyperChem™ 8.0.8 Molecular Modeling Software (Hypercube Inc., Gainesville, FL, USA) and ChemBio3D Ultra 11.0 (CambridgeSoft Corporation, Cambridge, UK). The decamer of acrylamide (polyacrylamide) was drawn using ChemBio3D Ultra in its syndiotactic stereochemistry as a 3D model, whereas the structures of CHT (10 glucosamine saccharide units) and pectin (10 galactopyranosyl uronic acid units) were built from standard bond lengths and angles using the polysaccharide Builder Module on HyperChem 8.0.8. The models were initially energy minimized using MM + force field and the resulting structures were once again energy minimized using the Amber 3 (assisted model building and energy refinements) force field. The conformer having the lowest energy was used to create the polymer–polymer complex. A complex of one polymer molecule with another was assembled by parallel disposition of the molecules and an identical procedure of energy minimization was repeated to generate the final models: CHT–HPAAm, pectin–HPAAm, and pectin–CHT–HPAAm. Furthermore, various energies and hydrogen bond lengths involved in the molecular interactions between CHT–HPAAm, pectin–HPAAm, and pectin–CHT–HPAAm were computed.

Physicomechanical Properties of the Polyelectrolyte Matrices

The physicomechanical properties of the matrices were evaluated in terms of their matrix resilience (MR), matrix hardness (MH), and deformation energy (DE). A calibrated texture analyzer (TA.XT*plus*, Stable Microsystems, Surrey, UK) fitted with a cylindrical steel probe (50 mm diameter; for MR) and a flat-tipped steel probe (2 mm diameter; for MH and DE) was employed. The parameters employed for the analysis is outlined in Table II. All studies (N=3) were conducted at room temperature (25°C).

MR (%) was calculated by the percentage of the ratio between the area under the curve (AUC) of the peak to baseline (after the force is removed; AUC_{2-3}) and the baseline to peak (before the force is removed; AUC_{1-2}) from a force–time profile (Fig. 1a). MH (N/mm^2) and DE (J) were both determined based on force–distance profiles, in particular, MH was elucidated from the gradient between the initial force and the maximum force attained, and DE from the AUC (Fig. 1b).

Table II. Textural Profiling Parameters Settings Employed for Physicochemical Characterization of the Polyelectrolyte Matrices

Parameters	MR[a] (%)	MH[b] (N/mm^2)	DE[c] (J)
Pre-test speed	1 mm/s	1 mm/s	1 mm/s
Test speed	0.5 mm/s	0.5 mm/s	0.5 mm/s
Post-test speed	10 mm/s	10 mm/s	10 mm/s
Trigger type	Auto	Auto	Auto
Trigger force	0.05 N	0.05 N	0.05 N
Load cell	5 kg	5 kg	5 kg
Compression strain	Variable	N/A	N/A
Target mode	Strain (40%)	Distance	Distance

[a] Matrix resilience
[b] Matrix hardness
[c] Deformation energy

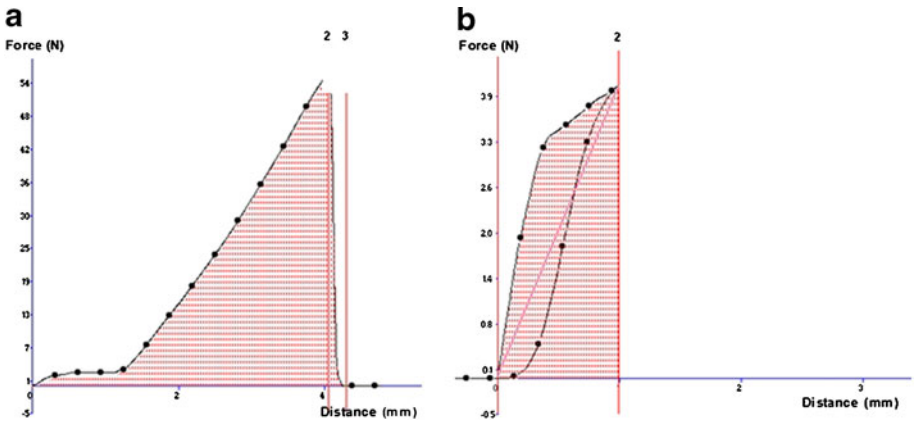

Fig. 1. Typical force–time and force–distance profiles of the polyelectrolyte matrices for determining **a** matrix resilience, and **b** matrix hardness (determined from gradient between anchors *1* and *2*) and deformation energy (determined from AUC between anchors *1* and *2*)

The Porositometric Characteristics of the Polyelectrolyte Matrices

Surface area and porosity analysis was performed on all polyelectrolyte matrices using a Porositometric Analyzer (Micromeritics ASAP 2020, Norcross, GA, USA). Samples were initially degassed to aid the removal of surface moisture and contaminants prior to analysis. Sample preparation briefly involved the weighing of each matrix (13×5 mm) with subsequent division of the matrices into quadrants capable of passing through the neck of the sample tube (I.D=9.53 mm). A glass filler rod was then inserted into the sample tube to reduce the total free space volume within the tube facilitating a reduction in the time required for complete degassing to occur. Samples were completely degassed after a period of between 7 and 9 h, the process of which encompassed an evacuation and heating phase. The respective parameter settings are shown in Table III.

Subsequent to complete degassing, the sample tube was transferred to the analysis port where data such as surface area, pore volume, and pore size was obtained in accordance with BJH and BET computations. The most widely used standard procedure for the determination of surface area of porous materials is based on the BET gas adsorption method which occurs in a two-stage process (37). Firstly, the BET equation was used in the linear form to determine the monolayer capacity based on Eq. 1.

$$\frac{p}{n^a(p^0-p)} = \frac{1}{n^a_m \times C} + \frac{(C-1)p}{n^a_m \times Cp^0} \tag{1}$$

Where, n^a refers to the quantity of N_2 adsorbed at the relative pressure P/P_0, $n^a{}_m$ was the monolayer capacity and C was exponentially related to the enthalpy of adsorption in the first adsorbed layer.

The surface area was then determined from the monolayer capacity using Eqs. 2 and 3 in the determination of the total and specific surface areas. This, however, required data regarding the molecular cross-sectional area a^m occupied by the adsorbate in the complete monolayer.

$$A_s(\text{BET}) = n^a_m \times L \times a_m \tag{2}$$

$$a_s(\text{BET}) = A_s(\text{BET})/m \tag{3}$$

Where A_s(BET) and a_s(BET) are the total and specific surface areas, respectively, of the adsorbent (of mass m) and L is the Avogadro constant.

Table III. Evacuation and Heating Phase Parameters Employed for Porositometric Analysis

Parameter	Rate/target
Evacuation phase	
Temperature ramp rate	10°C/min
Target temperature	40°C
Evacuation rate	50.0 mmHg/s
Unrestricted evacuation from	30 mmHg
Vacuum set point	500μmHg
Evacuation time	60 min
Heating phase	
Temperature ramp rate	10°C/min
Hold temperature	30°C
Hold time	900 min

Surface Morphological Analysis of the Polyelectrolyte Matrices

The surface morphology of the polyelectrolyte matrices were characterized by scanning electron microscopy (SEM; JSM-840 Scanning Electron Microscope, JEOL 840, Tokyo, Japan), at an accelerating voltage of 19 kV. This was performed to assess the surface characteristics of the matrices in relation to the nature and blend of polymers employed. Matrix samples were mounted on aluminum stubs and sputter-coated with a thin layer of gold palladium. Samples were then stored in a desiccator until analysis to avoid absorption of moisture onto the lyophilized matrices. Photomicrographs were captured at magnifications of ×1,400 and ×2,300.

Determination of the Drug Entrapment Efficiency

With the aim of ascertaining the quantity of DPH entrapped within each matrix, individual matrices ($N=3$) were finely triturated and subsequently dissolved in 100 mL of simulated gastric fluid (SGF; pH 1.2; 37°C). After complete dissolution, the solutions were filtered through a hydrophilic 0.45 μm Millipore membrane filter (Millipore® Millex-HV) (Millipore Corporation, Billerica, MA, USA) and analyzed spectroscopically (Lambda 25, UV/VIS Spectrometer, PerkinElmer®, Waltham, MA, USA) at a wavelength of 254 nm. The absorbances attained were then fitted to the relevant calibration curves ($R^2=0.996$) for the calculation of DPH content per matrix.

In vitro Drug Release Analysis from the Polyelectrolyte Matrices as a Function of Polymer Blends Employed

For *in vitro* evaluation of a controlled release drug delivery system, the ideal dissolution testing system should as close as possible mimic the *in vivo* conditions with regard to pH, types of enzymes present, fluid volume, and mixing intensity within the human gastrointestinal tract (38–40). However, such dissolution specifications are very difficult to be validated (38). For this reason, conventional methods are used and provide essential information about the functionality of the system design rather than its *in vivo* performance. To improve the relevance of the results obtained, a pH gradient and various transit times that closely resembles that of the gastrointestinal tract was employed. *In vitro* drug release studies were performed with a USP Bio-Dis® Apparatus (Caleva RRT 8; Caleva Ltd, Sturminster Newton, Dorset, England) at 37±0.5°C using 220 mL of test medium in each vessel, mesh sizes of 420 μm for both the top and bottom of the glass cylinders and a dip rate of 10 dpm for all experiments. Samples were removed at predetermined time-points and analyzed by UV spectroscopy (Lambda 25, UV/VIS Spectrometer, PerkinElmer®, Waltham, MA, USA) at a wavelength maximum of 254 nm ($N=3$). The pH differential employed included test media of: SGF (pH 1.2; 37°C; $R^2=0.996$) (41) for 2 h and simulated intestinal fluid (SIF; pH 6.8; 37°C) ($R^2=0.997$) (41) for the subsequent 4 h to complete the 6-h study period.

RESULTS AND DISCUSSION

Synthesis Validation of the Polyelectrolyte Matrices

Band shifts, changes in the peak intensity and peak broadening revealed by FTIR spectra of the various polymer blends in relation to the native polymers provided evidence that these modifications were specifically derived from chemical interactions and/or electrostatic interactions due to synthesis of the polyelectrolyte matrices. From the FTIR spectra of CHT, the presence of amine groups was substantiated by a broad band from 3,360 to 3,340 cm^{-1} signifying NH_2 stretching. The peak at 2,870 and 1,587 cm^{-1} was assigned to the C–H stretching and NH_2 deformation, respectively. The native PAAm was dominated by primary amide groups ($–CONH_2$) that essentially resulted in spectra indicating NH_2 stretching (3,400–3,150 cm^{-1}) and C = O stretching (1,680–1,660 cm^{-1}). Without the application of hydrolyzing agents, PAAm remained resistant to hydrolysis in aqueous solutions maintained at room temperature (42). However, with the inclusion of SPS to the polymeric blend partial alkaline hydrolysis of PAAm occurred. This resulted in the partial conversion of the amide groups to randomly distributed polar carboxyl groups carrying negative charges that rendered PAAm as a strong anionic polyelectrolyte. Furthermore, due to the employment of acetic acid as a solvent, the $–NH_2$ groups on the CHT molecule were converted to $–NH_3^+$ groups, resulting in the cationic nature of the polymer solution. Thus, a combination of these polymers results in an electrostatic attraction between the relevant oppositely charged polyions to form a PEC (43) as depicted in Fig. 2.

The corresponding FTIR spectra of these matrices revealed unique distinctive peaks between 1,425–1,390 cm^{-1} indicating the presence of $–COO^-$ symmetrical stretching and a distinctive peak at 1,535 cm^{-1} signifying $–NH_3^+$ deformation. These peaks essentially form the necessary validation for the formation of a PEC between CHT and HPAAm. However, there was still evidence of the presence of remaining amide groups from the non-hydrolyzed amide groups of HPAAm.

According to Liu *et al*. (44), typically at low ionization, polyacids function as hydrogen donors and can thus form intermolecular hydrogen bonds with the non-ionic PAAm, which is a proton acceptor, to form an intermolecular complex. In addition, the intermolecular interaction between a polyacid and PAAm is also dependent on the degree of ionization of the polyacid as well as the structural compatibility between the two polymers. Since PAAm was only partially hydrolyzed the numerous remaining $–NH_2$ groups present on the polymer backbone provided the basis for the electrostatic interaction with the $–COO^-$ groups of pectin in this study. The FTIR spectrum of these matrices revealed a predominant broad band between 2,500 and 3,500 cm^{-1} indicative of H-bonded OH stretching due to the free carboxylic groups of the HPAAm. However, the characteristic feature of these matrices was the disappearance of the peak at 1,590 cm^{-1} which signified NH_2 deformation of the primary amine groups. Reactions between anionic and cationic macromolecules in aqueous solutions lead to the formation of inter-polymeric complexes and since pectin and CHT are electrostatically complementary macromolecules, it is theorized that an electrostatic interaction between the positively charged amino groups at C-2 of the CHT pyranose ring and negatively charged carboxyl groups at C-5 of the pectin pyranose ring may have led to the formation of a PEC (45,46).

Based on FTIR spectra of pectin–CHT–HPAAm matrices relative to the spectra of CHT–HPAAm matrices, it was found that the spectra were identical except for the disappearance of the peak at 1,535 cm^{-1} in the pectin–CHT–HPAAm matrices. As described previously, this peak was indicative of NH_3^+ deformation. Thus, the existence of this peak in CHT–HPAAm matrices indicated a surplus of NH_3^+ sites due to the partial hydrolization of PAAm and thus an insufficient number of COO^- sites available for 'total' electrostatic interaction. However, the inclusion of pectin as part of the blend provided additional COO^- anionic sites that

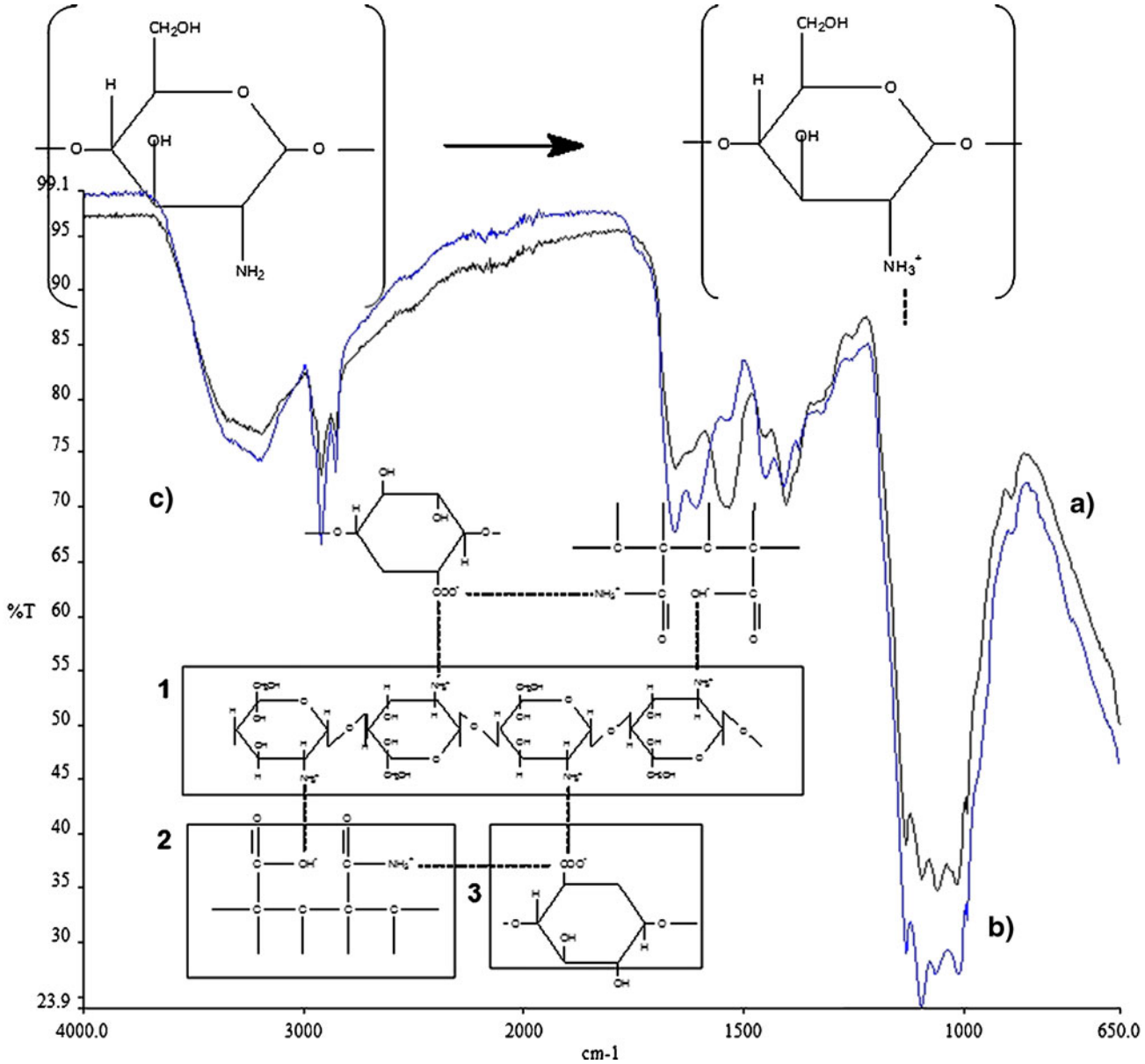

Fig. 2. FTIR spectra of **a** CHT–HPAAm matrices, and **b** pectin–CHT–HPAAm with inset **c** possible chemical structure of the electrostatic interaction between CHT, pectin, and HPAAm with (*1*) indicative of the CHT polymeric chain, (*2*) partially hydrolyzed PAAm, and (*3*) pectin

facilitated the electrostatic interaction between the NH_3^+ ions of CHT and the COO^- ions of pectin. In addition to these electrostatic interactions, a further interaction was observed between the remaining $–NH_2$ groups of HPAAm and the $–COO^-$ groups of pectin (Fig. 2).

Molecular Mechanistic Elucidation of Polyelectrolyte Complex Performance

In order to further support the synthesis validation and the FTIR results obtained, molecular mechanics simulations was undertaken in the form of energy minimizations to demonstrate electro- and structure-selective binding of saccharidic moieties, CHT, and pectin, to partially hydrolyzed PAAm. Molecular mechanics described the energy of the molecules in terms of a simplified function that accounted for distortion from ideal bond distances and angles, as well as for non-bonded Van der Waals and Coulombic interactions. The molecular tectonics of PECs in this study was found to be affected by various types of attractive interactions such as Van der Waals contacts, H-bonds, and electrostatic interactions. Table IV and Fig. 3 show the results of molecular mechanics computations performed in vacuum. The final conformation models of molecular networks were generated by the molecular mechanics computations for formable complex structures in relation to the cooperative ion-pair binding between the carboxyl ($–COO^-$) and the protonated amine ($–NH_3^+$) groups. The strong binding affinity in CHT–HPAAm was due to the electrostatic interaction caused by the $–NH_3^+$ and $–COO^-$ ions that proceed in accordance with the short-range Van der Waal attractions and secondary interactions such as H-bonding. In contrast, $–COO^-$ ions of

Table IV. Computed Energy Parameters (kcal/mol) of the Polyelectrolyte Complexes Formed Between Chitosan, HPAAm, and Pectin

Structure	Energy (kcal/mol)						
	Total	Bond	Angle	Dihedral	VDW	H bond	Elec
CHT	35.556	3.12011	18.035	25.7749	13.3231	0	−24.6973
Pectin	−7.560326	5.03147	24.4993	28.571	29.0303	0	−94.6923
HPAAm	10.356753	1.42469	5.46554	8.57397	−5.07248	−0.03497	0
CHT–HPAAm	13.129162	5.85083	27.9893	42.3994	−31.8998	−0.576249	−29.7597
Pectin–HPAAm	−34.25015	7.5611	36.3226	46.28	−28.8202	−0.074842	−95.5188
Pectin–CHT–HPAAm	−79.08684	10.8678	57.0293	68.2813	−48.8639	−1.45089	−165.825

pectin interacted with the $-NH_3^+$ of HPAAm. Although the pectin–HPAAm complex was electrostatically more stable than CHT–HPAAm, the $E_{elec(CHT-HPAAm-CHT)}$ and $E_{elec(pectin-HPAAm-pectin)}$ were computed to be 5 and 1 kcal/mol, respectively, indicating that the electrostatic interactions in pectin–HPAAm complexes were weaker than the interactions in the CHT–HPAAm complexes. Hence, HPAAm was playing a dual role as an anionic electrolyte in the presence of CHT and a cationic polysaccharide in the vicinity of pectin. Interestingly, the Van der Waals energy was more stabilized in the case of pectin–HPAAm (decreased by 58 kcal/mol) than in CHT–HPAAm (44 kcal/mol) which demonstrated the significance of a structural backbone fit between the host and guest molecule. In addition, pectin–HPAAm was more stabilized by H-bonds as shown in Table IV and Fig. 3a–c.

Finally, these complex interactions were also explored through the pectin–CHT–HPAAm complex and observed the formation of a PEC represented by a novel tri-polymeric ionic-quadrilateral (TPIQ) consisting of $-NH_3^+$ ions of CHT, $-COO^-$ ions of pectin and $-NH_3^+$, and $-COO^-$ ions of HPAAm as shown in the FTIR spectra of Fig. 2. Figure 3c clearly demonstrates the polyelectrolyte selection of the pectin–CHT, pectin–HPAAm, and CHT–HPAAm polymers. Figure 3c also depicts the energy minimized structures of pectin–CHT–HPAAm where due to the flexibility of the polymer chain, the relevant segments of polymers orientated their configuration to form a remarkable structure fit between the $-NH_3^+$ and $-COO^-$ ions, the electrostatic, Van der Waals and H-bond interactions being pseudo-optimized. Comparison of the complexes revealed that the pectin–CHT–HPAAm complex was superiorly stable in total energy, Van der Waals, H-bond and electrostatic interactions by 92, 17, 0.88, and 136 kcal/mol, respectively, in comparison to CHT-HPAAm and 45, 20, 1.38, and 70 kcal/mol, respectively, in comparison to pectin–HPAAm. The difference in the electrostatic interactions of the TPIQ and the biopolymer complexes of approximately 136 and 70 kcal/mol suggested that the complex was stabilized mainly by Coulombic attractions (Table IV) and supported by the Van der Waals forces with a difference of 17 and 20 kcal/mol, respectively. Although their H-bond lengths ranged from 2.1579 to 3.1772A° (Fig. 3d) and may be considered as H-bonds of medium strength, it is likely that these interactions may be significant for the stability of the TPIQ. Therefore, the highly stable structure of TPIQ was due to the formation of a pectin-CHT PEC in the vicinity of HPAAm which again demonstrated the significance of a structural backbone fit due to the superior fit between the location of the positive charges and the position of the negatively charged groups.

Physicomechanical Analysis of the Polyelectrolyte Matrices

MR was employed as a measure of the cohesiveness of the polyelectrolyte matrices and referred to the ability of the matrices to recover to their original dimensions after a compressive stress was applied by the textural probe (47). It was determined that at a consistent strain of 40%, the CHT–HPAAm matrices proved to be the most resilient at 6.1± 0.03%, compared to pectin–HPAAm matrices with a resilience of 5.3±0.02% (Fig. 4). According to Platé (48), on forming a complex, the reacting chains of components of a PEC lose their flexibility and intermolecular mobility. Considering that pectin–CHT–HPAAm matrices had additional electrostatic interactions between CHT–pectin and pectin–HPAAm, along with the interaction between CHT and HPAAm, it was thus warranted that these matrices would have the least resilient nature.

The energy required to overcome the adhesive and cohesive forces within the matrices is regarded as the deformation energy. As expected, the energy dissipated in the causation of this effect was markedly lower for pectin–CHT–HPAAm matrices compared to the other variants. Furthermore, the MH of pectin–CHT–HPAAm matrices was lower than pectin–HPAAm matrices and CHT–HPAAm matrices (Fig. 4).

The MR and MH are pertinent physicomechanical properties that corroborate the matrices potential to absorb energy during the fluid imbibitions process with drug release, the physical matrix stability, and swelling or erosion behavior for controlling the drug release behavior. In this study, MR was represented as an index of energy absorption, while MH was an index of resistance against deformation. In the case of the pectin–CHT–HPAAm matrices, the orientation of structure and density closely controlled these properties to display the anomalous behavior that was attributed to matrix curing and the production of a ‘deforming-type’ matrix. The effect of polymer blend ratios can also not be ignored as they imparted various intricate physicomechanical characteristics. The MH therefore also decreased with decreasing MR. When the textural probe impacted the matrix, the MR decreased with relatively softer matrices. This confirmed the plastic deformation of the matrices. In other words, the matrices absorbed more impacting energy with softer matrices and therefore the MR was poor. These results suggest that the MR and MH are

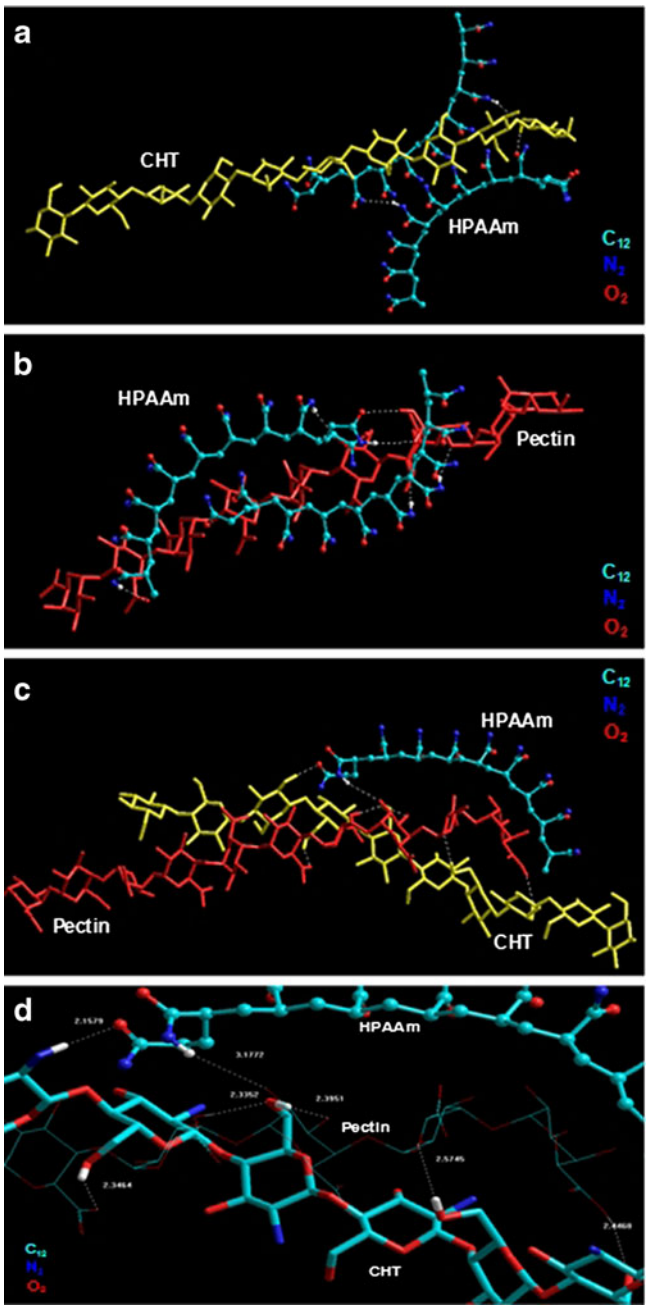

Fig. 3. Energy minimized geometrical preferences of the polyelectrolyte complexes derived from molecular mechanics calculations: **a** CHT–HPAAm, **b** pectin–HPAAm, **c** pectin–CHT–HPAAm complex, and **d** H-bond lengths (Å) involved in the pectin-CHT–HPAAm complex as computed via AMBER force field. The color codes for elements C_{12}, N_2, and O_2 are also shown

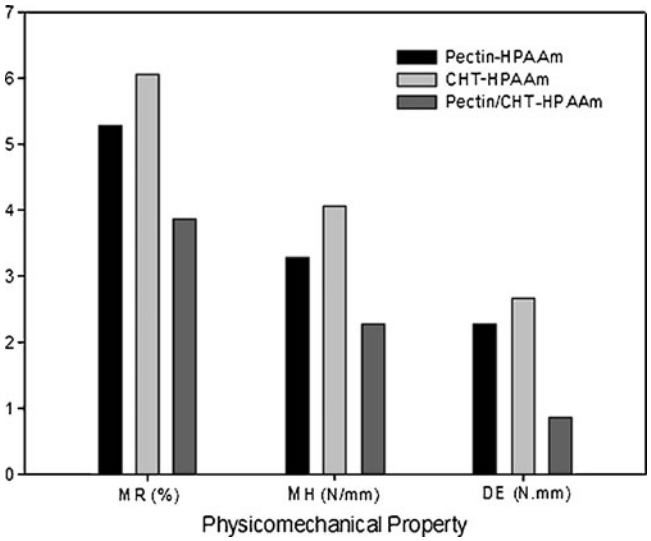

Fig. 4. Physicomechanical properties of the polyelectrolyte matrices produced from different polymer blends

potentially governed by non-linear deformation kinetics and anomalous physicomechanical mechanisms due to the polyelectrolyte complex formation.

Influence of the Polymer Blend on the Porositometric Properties of the Polyelectrolyte Matrices

The technique of physical gas adsorption was used for assessing the pore characteristics of the various polyelectrolyte matrices as a direct measure of its porous properties and structure (49). When applied over a wide range of relative pressures (P/P_0), N_2 adsorption isotherms provided critical data on the pore size distributions in terms of their micro-, meso-, and macropore ranges (±0.5–200 nm). The BJH model of determining pore volume and pore size distribution in the mesopore and macropore range was based on the Kelvin equation and corrected for multi-layer adsorption (36). Several assumptions were made with the BJH pore size distribution computation, namely pores were rigid and of a well-defined shape, the distribution was confined to the mesopore range and filling/emptying of pores did not depend on the location. It was generally considered that matrices that were purely mesoporous and comprised non-intersecting mesopores of cylindrical geometry and similar size exhibited type IV isotherms with a type H1 hysteresis loop (49). However, due to the random distribution of pores and an interconnected pore system of the matrices, the hysteresis loop was of type H2 or H3. Figure 5 provides an illustration of typical isotherms and hysteresis models employed.

The isotherm of pectin–CHT–HPAAm matrices (Fig. 6a) was typical of a type IV isotherm accompanied by a H3 hysteresis. The characteristic hysteresis loop was associated with capillary condensation that took place in mesopores. This was supported by data obtained where the pore sizes of the matrices were found to be 22.46 nm according to the desorption curve of the isotherm. Furthermore, according to the isotherm, a forced closure of the hysteresis occurred at $P/P_0>0.45$ which was due to a sudden drop in the volume of N_2 adsorbed along the desorption curve. This phenomenon was referred to as the tensile strength effect. The isotherm increased rapidly near $P/P_0=1$ that was indicative of the presence of macropores with a significant vertical rise signifying the large diameters of the macropores.

In contrast, pectin–HPAAm matrices exhibited an isotherm not characteristic of any isothermic types according to the IUPAC classification system. However, certain regions of the isotherm were similar to that of a type IV isotherm accompanied with a H4 hysteresis loop (Fig. 6b). According

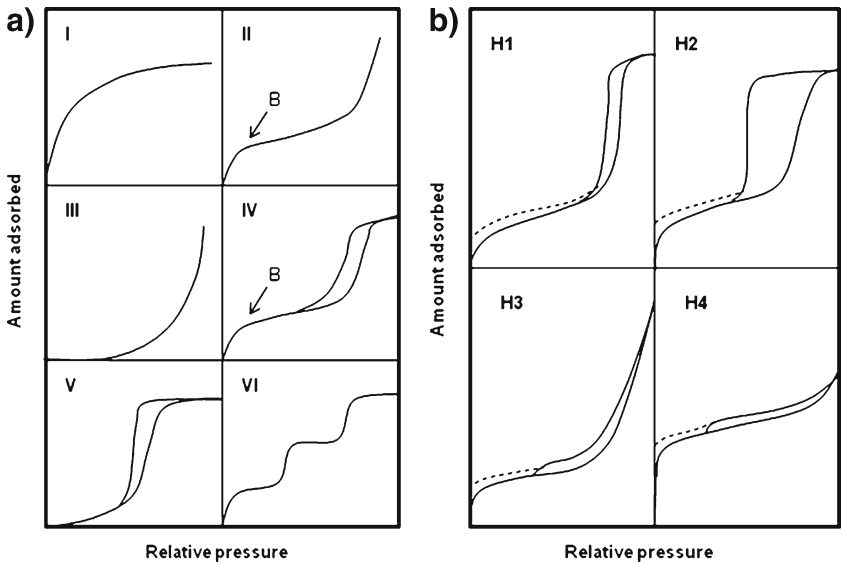

Fig. 5. Schematics depicting **a** types of isotherms and **b** types of hysteresis loops according to the IUPAC classification system (adapted from Sing *et al.* (37))

to the data obtained pectin–HPAAm matrices had a pore size of 5.15 nm based on the desorption isotherm. This was within the mesopore range and explained the presence of the H4 hysteresis of the isotherm. Furthermore, the presence of a low pressure hysteresis (P/P_0<0.45) suggested that micropores were also present in the matrices. However, Groen *et al.* (49) described that a high degree of mesoporosity may lead to a higher mesopore surface area, and this can in turn significantly affect the low-pressure region (micropore range) of the isotherm. This explanation is validated by the elevated surface area of the matrices despite the smaller pore sizes compared to the pectin–CHT–HPAAm and CHT–HPAAm matrices (Table V).

CHT–HPAAm matrices exhibited a similar isotherm to that of pectin–CHT–HPAAm matrices, with similar pore sizes (Table V). However, it deviated from the pectin–CHT–HPAAm matrices with its reduced surface area due to the reduced number of pores present in the matrix.

SEM micrographs of all matrices showed highly porous surface characteristics. Surface area and porosity studies suggested that the porosity of the matrices followed a random distribution and an interconnected pore system. This was evidenced from SEM images at various magnifications for each matrix formulation (Fig. 6). According to a type II and type IV isotherm, the point marked 'B' on Fig. 5 refers to the point at which monolayer adsorption was complete and was visible at the beginning of the almost linear mid-section of the isotherm. This point was clearly visible as a 'sharp knee' in the isotherm when $C \approx 100$ (Eq. 1). However, when C<20 this point was not present as a single point on the isotherm (50). Pectin–CHT–HPAAm matrices exhibited a type IV isotherm with no discernable point 'B' that correlated with its C value

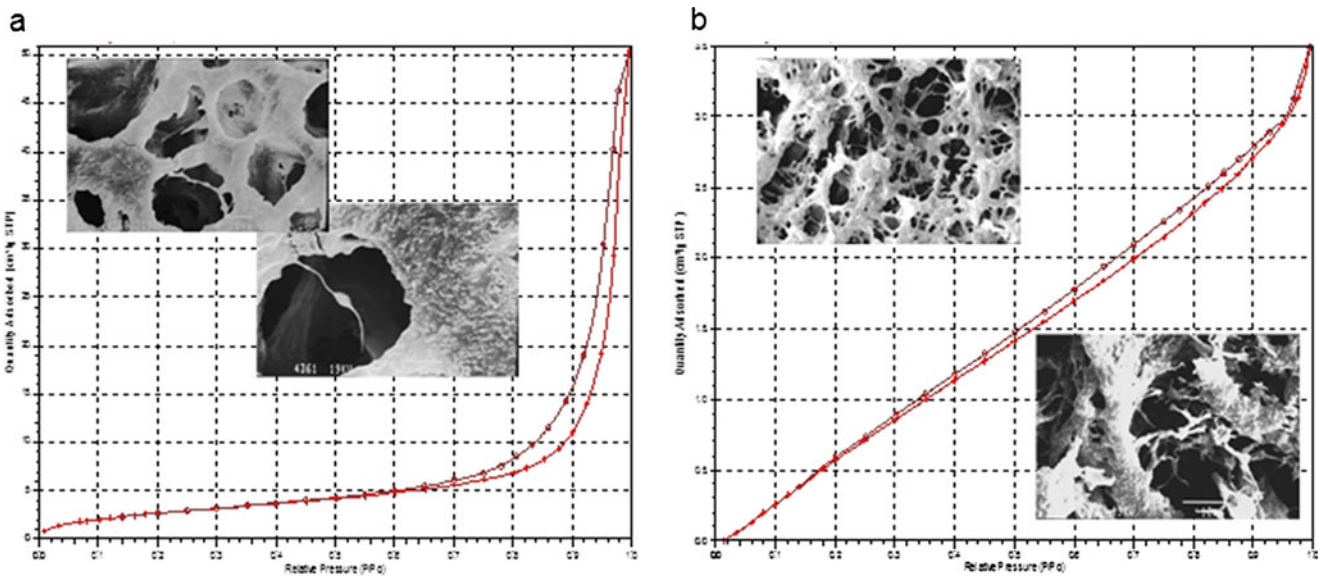

Fig. 6. Linear isothermic plots of **a** pectin–CHT–HPAAm matrices and **b** pectin–HPAAm matrices with insets of SEM micrograph images at magnifications of ×1,400 and ×2,300

Table V. Surface Area and Porosity Characteristics of the Various Polyelectrolyte Matrices

	Surface area (m^2/g)	Pore volume (cm^3/g)		Pore size (nm)	
	BET	A[a]	B[b]	A[a]	B[b]
CHT–HPAAm	2.70	0.021	0.021	26.069	21.647
Pectin–HPAAm	22.67	0.005	0.005	5.425	5.152
Pectin–CHT–HPAAm	10.50	0.078	0.078	25.379	22.462

[a] BJH adsorption branch
[b] BJH desorption branch

of 28.19. CHT–HPAAm matrices also had no discernible point 'B' with a *C* value of 12.16. This difference in the enthalpy of adsorption resulted in the difference in the surface areas of these matrices.

Effect of the Polymer Blend on the Drug Release Performance of the Polyelectrolyte Matrices

It has been reported that pore diameter may have a significant effect on the rate of drug release and can also affect the migration of the drug from the matrix into the release media (50). However, such a relationship between pore diameters and release rate is not always apparent. In addition to pore diameter, the number of pores may also be an important factor in controlling the release rate of drug from matrices.

Drug release data indicated a marked difference in the release profiles of the various polyelectrolyte matrices each containing 35 mg of DPH, particularly in the first 2 h under simulated gastric conditions. Each of these matrices was round with a diameter of 13 mm and a height of 5 mm (Fig. 7b). In this time, no drug was released from the CHT–HPAAm matrices, whereas 28.2% and 82.2% of DPH was released from the pectin–HPAAm and pectin–CHT–HPAAm matrices, respectively. After 4 h of dissolution in simulated intestinal conditions, complete drug release was achieved from the pectin–CHT–HPAAm matrices in contrast to only 35.0% release from CHT–HPAAm matrices (Fig. 7a). The pH differential employed, simulating conditions of the gastric and small intestinal environments, showed that CHT–HPAAm matrices exhibit applicability in drug delivery of pharmaceutical agents in regions of the small intestine and colon as no drug was released in the gastric region. This modulated release profile would prove to be beneficial for the localized treatment of chronic conditions such as ulcerative colitis where distal small intestinal and colonic inflammation is prevalent. In contrast, since pectin–HPAAm matrices exhibited controlled release of DPH in SGF and SIF with <40% released, it may still allow for an almost 60% delivery of drug in the colonic region and thus may be beneficial for the treatment of Crohn's disease where the entire gastrointestinal tract is inflamed. The drug release data complements results obtained from the surface area and porosity studies. The surface area (m^2/g) of CHT–HPAAm matrices was significantly lower than that of the other matrices (2.7 *vs.* 22.7 and 10.5 m^2/g, respectively). The lower surface area sustained the absorption of dissolution media into the matrix thus reducing the swelling rate and subsequently the rate of DPH diffusion out of the matrix. On the contrary, despite the lower surface area of pectin–CHT–HPAAm matrices compared to pectin–HPAAm matrices, the rate of drug release was still higher. This finding may be supported by the higher pore volume and pore sizes as well as the presence of macropores in the pectin–CHT–HPAAm matrices compared to pectin–HPAAm matrices.

CONCLUSIONS

Many approaches currently exist for the development of composite polymer materials that may be used for modulating

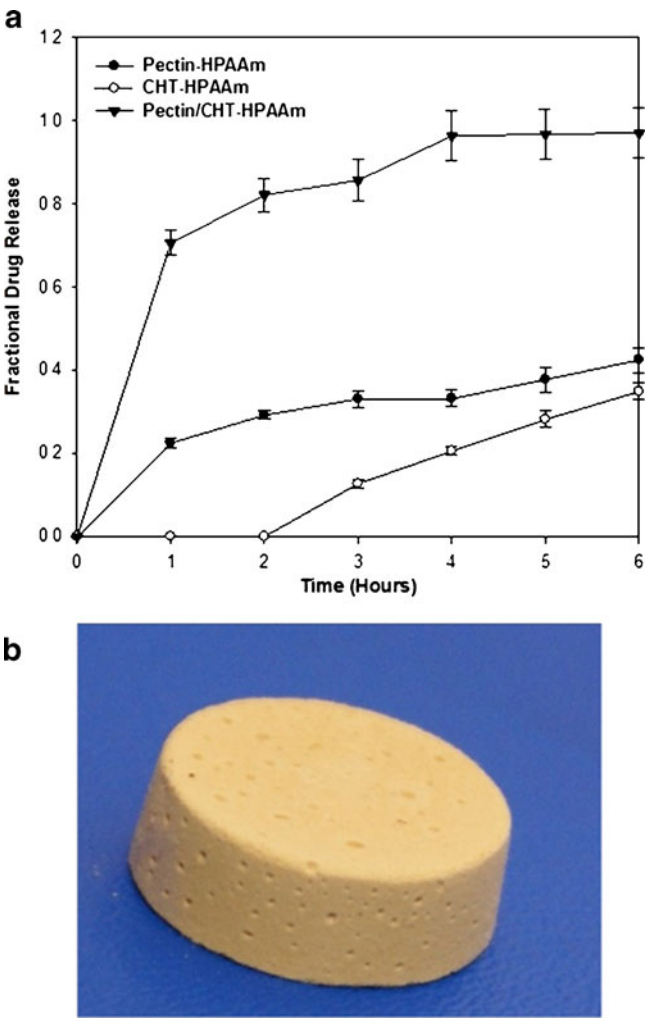

Fig. 7. **a** Drug release profiles obtained for polyelectrolyte matrices in conditions simulating the gastrointestinal tract (N=3, SD<0.06 in all cases) and **b** a digital image depicting the matrices produced

drug release. One such method evaluated in this study focused on the formulation of polyelectrolyte complexes between natural polysaccharide polymers and a hydrolyzed synthetic polymer. The interaction between partially hydrolyzed PAAm molecules to both anionic (pectin) and CHT polyelectrolytes formed three polymer complexes accommodated by electrostatic, van der Waals, and H-bond interactions. The polyelectrolyte matrices demonstrated controlled release of the highly water-soluble model drug, DPH. Drug release behavior was pivoted to the porositometric properties of the various matrices. It was found that by modifying the concentrations of the polymers employed (CHT, pectin, and PAAm) and the combinations thereof, the applicability of these matrices may be accentuated for effective site-specific and controlled oral drug delivery applications.

ACKNOWLEDGMENTS

This research was supported by the National Research Foundation of South Africa and the Technology Innovation Agency of South Africa.

REFERENCES

1. Yu L, Dean K, Li L. Polymer blends and composites from renewable resources. Prog Polym Sci. 2006;31:576–602.
2. Xiao C, Weng L, Lu Y, Zhang L. Blend films from chitosan and polyacrylamide solutions. J Macromol Sci Pure Appl Chem. 2001;A38:761–71.
3. Coombes AGA, Verderio E, Shaw B, Li X, Griffin M, Downes S. Biocomposites of non-crosslinked natural and synthetic polymers. Biomater. 2002;23:2113–8.
4. Barnes CP, Sell SA, Boland ED, Simpson DG, Bowlin GL. Nanofiber technology: designing the next generation of tissue engineering scaffolds. Adv Drug Deliv Rev. 2007;59:1413–33.
5. Li X, Liu KL, Wang M, Wong SY, Tjiu WC, He CB, *et al*. Improving hydrophilicity, mechanical properties and biocompatibility of poly[(R)-3-hydroxybutyrate-co-(R)-3-hydroxyvalerate] through blending with poly[(R)-3-hydroxybutyrate]-alt-poly(ethylene oxide). Acta Biomater. 2009;5:2002–12.
6. Pedram MY, Retuert J, Quijada R. Hydrogels based on modified chitosan, I: synthesis and swelling behavior of poly(acrylic acid) grafted chitosan. Macromol Chem Phys. 2000;201:923–30.
7. Reis AV, Guilherme MR, Cavalcanti OA, Rubira AF, Muniz EC. Synthesis and characterization of pH-responsive hydrogels based on chemically modified Arabic gum polysaccharide. Polym. 2006;47:2023–9.
8. Derkaoui SM, Avramoglou T, Barbaud C, Letourneur D. Synthesis and characterization of a new polysaccharide-graft-polymethacrylate copolymer for three-dimensional hybrid hydrogels. Biomacromolecules. 2008;9:3033–8.
9. Lee KY, Park WH, Ha WS. Polyelectrolyte complexes of sodium alginate with chitosan or its derivatives for microcapsules. J Appl Polym Sci. 1997;63:425–32.
10. Simsek-Ege FA, Bond GM, Stringer J. Polyelectrolyte complex formation between alginate and chitosan as a function of pH. J Appl Polym Sci. 2003;88:346–51.
11. Lammertz S, Grünfelder T, Ninni L, Maurer G. A model for the Gibbs energy of aqueous solutions of polyelectrolytes. Fluid Phase Equilib. 2009;280:132–43.
12. Lee SB, Lee YM, Song KW, Park MH. Preparation and properties of polyelectrolyte complex sponges composed of hyaluronic acid and chitosan and their biological behaviors. J Appl Polym Sci. 2003;90:925–32.
13. Chellat F, Tabrizian M, Dumitriu S, Chornet E, Magny P, Rivard CH, *et al*. *In vitro* and *in vivo* biocompatibility of chitosan–xanthan polyionic complexes. J Biomed Mater Res. 2000;51:107–16.
14. Peniche C, Argüelles-Monal W. Chitosan based polyelectrolyte complexes. Macromol Symp. 2001;168:103–16.
15. Shchipunov YA, Postnova IV. Water-soluble polyelectrolyte complexes of oppositely charged polysaccharides. Compos Interfaces. 2009;16:251–79.
16. Macleod GS, Collett JH, Fell JT. The potential use of mixed films of pectin, chitosan and HPMC for bimodal drug release. J Control Release. 1999;58:303–10.
17. Nichifor M, Lopes S, Bastos M, Lopes A. Self-aggregation of amphiphilic cationic polyelectrolytes based on polysaccharides. J Phys Chem B. 2004;108:16463–72.
18. Nagahata M, Nakaoka R, Teramoto A, Abe K, Tsuchiya T. The response of normal human osteoblasts to anionic polysaccharide polyelectrolyte complexes. Biomater. 2005;26:5138–44.
19. Sarmento B, Ribeiro A, Veiga F, Ferreira D. Development and characterization of new insulin containing polysaccharide nanoparticles. Colloids Surf B. 2006;53:193–202.
20. Argin-Soysal S, Kofinas P, Lo YM. Effect of complexation conditions on xanthan–chitosan polyelectrolyte complex gels. Food Hydrocolloids. 2009;23:202–9.
21. Lipp D, Kozakiewicz J, In: Kroschwitz JI, Howe-Grant M, Bickford M, Gray L, Editors. Kirk-othmer encyclopedia of chemical technology, 4th edn. New York: Wiley; 1991 (1). p. 266.
22. Sharma A, Desai A, Ali R, Tomalia D. Polyacrylamide gel electrophoresis separation and detection of polyamidoamine dendrimers possessing various cores and terminal groups. J Chromatogr A. 2005;1081:238–44.
23. Entry JA, Sojka RE, Hicks BJ. Carbon and nitrogen stable isotope ratios can estimate anionic polyacrylamide degradation in soil. Geoderma. 2008;145:8–16.
24. Yan LJ, Forster MJ. Resolving mitochondrial protein complexes using nongradient blue native polyacrylamide gel electrophoresis. Anal Chem. 2009;389:143–9.
25. Volk H, Friedrich RE. In: Davidson RL, editor. Handbook of water-soluble guns and resins. New York: McGraw-Hill; 1980. p. 16.
26. Zeynali ME, Rabbii A. Alkaline hydrolysis of polyacrylamide and study on poly(acrylamide-co-sodium acrylate) properties. Iran Polym J. 2002;11:269–75.
27. Kurenkov VF, Hartan HG, Lobanov FI. Alkaline hydrolysis of polyacrylamide. Russ J Appl Chem. 2001;74:543–54.
28. Sokker HH, Abdel Ghaffar AM, Gad YH, Aly AS. Synthesis and characterization of hydrogels based on grafted chitosan for the controlled drug release. Carbohydr Polym. 2009;75:222–9.
29. Krayukhina MA, Samoilova NA, Yamskov IA. Polyelectrolyte complexes of chitosan: formation, properties and applications. Russ Chem Rev. 2008;77:799–813.
30. Wakerly Z, Fell JT, Attwood D, Parkins DA. *In vitro* evaluation of pectin-based colonic drug delivery systems. Int J Pharm. 1996;129:73–7.
31. Macleod GS, Fell JT, Collett JH, Sharma HL, Smith AM. Selective drug delivery to the colon using pectin:chitosan: hydroxypropyl methylcellulose film-coated tablets. Int J Pharm. 1999;187:251–7.
32. Ahrabi SF, Madsen G, Dyrstad K, Sande SA, Graffner C. Development of pectin matrix tablets for colonic delivery of model drug ropivacaine. Eur J Pharm Sci. 2000;10:43–52.
33. Liu L, Fishman ML, Kost J, Hicks KB. Pectin-based systems for colon-specific drug delivery via oral route. Biomater. 2003;24:3333–43.
34. Maestrelli F, Cirri M, Corti G, Mennini N, Mura P. Development of enteric-coated calcium pectinate microspheres intended for colonic drug delivery. Eur J Pharm Biopharm. 2008;69:508–18.
35. Bernabé P, Peniche C, Argüelles-Monal W. Swelling behavior of chitosan/pectin polyelectrolyte complex membranes, effect of thermal cross-linking. Polym Bulletin. 2005;55:367–75.
36. Barret EP, Joyner LG, Halenda PH. Determination of pore volume and area distribution in porous substances. I. Computation from nitrogen isotherms. J Am Chem Soc. 1951;73:373–80.
37. Sing KSW, Everett DH, Haul RAW, Moscou L, Pierotti RA, Rouquerol J, *et al*. Reporting physisorption data for gas/solid systems with special reference to the determination of surface area and porosity. Pure Appl Chem. 1985;57:603–19.
38. Chambin O, Dupuis G, Champion D, Voilley A, Pourcelot Y. Colon-specific drug delivery: influence of solution reticulation

properties upon pectin beads performance. Int J Pharm. 2006;321:86–93.
39. Yang L, Chu JS, Fix JA. Colon-specific drug delivery: new approaches and *in vitro/in vivo* evaluation. Int J Pharm. 2002;235:1–15.
40. Hébrard G, Hoffart V, Cardot J-M, Subirade M, Alric M, Beyssac E. Investigation of coated whey protein/alginate beads as sustained release dosage form in simulated gastrointestinal environment. Drug Dev Ind Pharm. 2009;35:1103–12.
41. Lee SS, Lim CB, Pai, CM, Lee SP, Seo MG, Park H. Composition and pharmaceutical dosage form for colonic drug delivery using polysaccharides US Patent: 6,413,494. 1999. http://www.pharmcast.com/Patents/Yr2002/July2002/070202/6413494_Colonic070202.htm. Accessed on: May 10, 2010.
42. Veitser YI, Mints DM. Macromolecular flocculants in processes of natural water and wastewater treatment. Moscow: Stroiizdat; 1984.
43. Cao J, Tan Y, Che Y, Ma Q. Fabrication and properties of superabsorbent complex gel beads composed of hydrolyzed polyacrylamide and chitosan. J Applied Poly Sci. 2010;116(6):3338–45.
44. Liu L, Cooke PH, Coffin DR, Fishman ML, Hicks KB. Pectin and polyacrylamide composite hydrogels: effect of pectin on structural and dynamic mechanical properties. J Appl Polym Sci. 2003;92:1893–901.
45. Rashidova SS, Milusheva RY, Semenova LN, Mukhamedjanova MY, Voropaeva NL, Vasilyeva S. Characteristics of interactions in the pectin–chitosan system. Chromatographia. 2004;59:779–82.
46. Tripathi S, Mehrotra GK, Dutta PK. Preparation and physicochemical evaluation of chitosan/poly(vinyl alcohol)/pectin ternary film for food-packaging applications. Carbohydr Polym. 2010;79:711–6.
47. Pillay V, Fassihi R. *In vitro* release modulation from crosslinked pellets for site-specific drug delivery to the gastrointestinal tract: II. Physicochemical characterization of calcium–alginate, calcium–pectinate and calcium–alginate–pectinate pellets. J Control Release. 1999;59:243–56.
48. Platé NA. Problems of polymer modification and the reactivity of functional groups of macromolecules. Pure Appl Chem. 1976;46:49–59.
49. Groen JC, Peffer LAA, Ramırez JP. Pore size determination in modified micro- and mesoporous materials. Pitfalls and limitations in gas adsorption data analysis. Microporous Mesoporous Mater. 2003;60:1–17.
50. Jelvehgari M, Siahi-Shadbad MR, Azarmi S, Martin GP, Nokhodchi A. The microsponge delivery system of benzoyl peroxide: Preparation, characterization and release studies. Int J Pharm. 2006;308:124–32.